Il presente lavoro è stato pubblicato su Sensors & Actuators: B. Chemical 274, 2018, 210-217 con doi: https://doi.org/10.1016/j.snb.2018.07.128

Enhanced stability of Organic Field-Effect Transistor biosensors bearing electrosynthesized ZnO Nanoparticles

Rosaria Anna Picca[‡, a], *Kyriaki Manoli*[‡, a], *Antonio Luciano*[a], *Maria Chiara Sportelli*[a], *Gerardo Palazzo*[a], *Luisa Torsi*[*, a,b], *Nicola Cioffi**[, a]

[a] Dipartimento di Chimica, Università degli Studi di Bari "Aldo Moro", via E. Orabona 4 – 70126 Bari, Italy.

[b] The Faculty of Science and Engineering, Åbo Akademi University, Biskopsgatan 8 Åbo 20500, Turku, Finland.

[*]**Corresponding Authors**: nicola.cioffi@uniba.it , luisa.torsi@uniba.it

Telephone number: +390805442020; FAX: +390805442026

[‡]These authors contributed equally to this work.

Abstract: Herein electrosynthesized ZnO nanoparticles (ZnO NPs) agents to largely improve functional bio-interlayer organic field-effect transistor (FBI-OFET) biosensors stability are investigated. For a proof-of-principle, streptavidin (SA) was chosen as the capturing biomolecule to sense biotin and poly-3-hexylthiophene (P3HT) served as channel material. The ZnO NPs were prepared and integrated into the FBI-OFET architecture by means of a straightforward and versatile procedure. To this end, ZnO

NPs were mixed with an SA solution and the resulting aqueous suspension was readily spin-coated onto the SiO_2 gate dielectric. The P3HT film was spin-coated on the SA-ZnO NPs layer afterwards with the whole fabrication procedure taking no more than 30 min. The FBI-OFET biosensors bearing the ZnO NPs exhibited a shelf life exciding one year, while the bare ones failed to work after few weeks. Moreover, the ZnO NPs enabled a two orders of magnitude increase in field-effect mobility while the already proven very good sensing performances were retained. The electrical and XPS characterization of the ZnO NPs based functional bio-interlayer, provided information about the role of the nanostructured oxide on the improved device stability and a plausible mechanism for this occurrence is derived accordingly.

Keywords: zinc oxide; functional bio-interlayer; field–effect transistor sensors; extended lifetime; poly-(3-hexylthiophene)

1. Introduction

Bioelectronics, encompassing the integration of electronic components with biological elements, is a continuously expanding field that offers not only a stimulating interdisciplinary scientific arena but also interesting and potentially extremely useful applications in the clinical field [1]. Organic field-effect transistors (OFETs) [2,3] and their bioelectronic counterpart are becoming a relevant class of label-free sensing devices known for being highly sensitive selective and low-cost [4,5]. Among the

several architectures proposed so far, back-gated OFET involving a functional bio-interlayer (FBI) sandwiched between a solid insulating dielectric and the organic semiconductor (OSC) film, have successfully served as selective biosensors capable to detect down to low picomolar, pM (10^{-12} mole L^{-1}) levels [5,6]. The main advantage of this assembly relies on the occurrence that the recognition event takes place directly at the interface between the dielectric and OSC layer, namely at the interface where the amplified two-dimensional electronic transport takes place. By this means, the capturing biomolecules after the interaction with their affinity ligand undergo modifications that can directly impact on the OFET transport properties [7–9]. A proof-of-concept of such a technology was provided by depositing streptavidin (SA) as bio-recognition layer in an FBI-OFET based on P3HT for biotin detection [7,10].

Despite their very high sensitivity, the stability of sensing FET devices integrating a biological component may be limited over time and upon use, especially when the monitoring of specific (bio)markers has to be pursued in physiological environments. Moreover, operational stability of the P3HT film (and OSCs in general) may be questionable due to degradation caused by moisture and air [11,12]. Indeed, the stability is among the biggest hurdle in developing OFETs for real-life applications and there have been numerous reports for extending the lifetime of P3HT based OFETs with controlled exposure to nitrogen and/or argon flow and encapsulation [13,14]. While these issues have been widely explored [12,15] as yet, the exact degradation mechanisms of P3HT is still under debate although it is consistently correlated to

absorption of oxygen or water. Seo *et al.* for instance studied the effect of water vapor on P3HT films by means of X-ray photoelectron spectroscopy (XPS) [16], proving how H_2O is responsible for the partial oxidation of P3HT.

Improving the analytical performance is a general goal in (bio)sensor development, which is often pursued by implementing inorganic nanomaterials in the device structure [17–19]. Hybrid composites containing nanomaterial components have received increasing attention for the fabrication of advanced sensing layers: membranes consisting of poly-vinyl-alcohol and ionic liquid doped with WO_3 nanoparticles (NPs) were employed in H_2S gas sensors [20]; flexible polyaniline/carbon nanotube films were sensitive to NH_3 [21]; reduced graphene oxide-carboxylated polypyrrole nanotube hybrids were combined with glucose oxidase in a FET glucose biosensor [22]. Among nanomaterials, ZnO nanostructures are particularly appealing for their electrical properties, low toxicity and biocompatibility [23,24], making them suitable candidates to be used in electronic devices [25,26]and FET biosensors [27,28]. Blends or bilayers of n-type ZnO nanophases with p-type OSCs, such as ZnO/pentacene [25], ZnO/polyfluorene [29], ZnO/poly(3-hexylthiophene) [30–32], have shown enhanced electrical properties as compared to the bare OSC films. Interestingly however, n-type ZnO nanowires or nanorods have been mainly engaged in the development n-type FET biosensors [27,33]. In the elicited cases, the chemical functionalization procedures are often exploited to achieve improved immobilization of the biological recognition elements on the ZnO structures. Typically, these protocols consist of several steps, such

as for instance: ZnO surface activation, silanization, glutaraldehyde modification for biomolecule adhesion [27,34].

In this work, the integration of electroproduced ZnO nanoparticles (ZnO NPs) in a FBI-OFET biosensor, addressed as P3HT/SA-ZnO NPs FBI-OFET, was investigated as an easy and effective means to extend the bioelectronic device lifetime, enhancing the field-effect mobility by two orders of magnitude, without altering its already remarkable sensing performance falling in the low pM range [7,10]. SA-biotin couple was selected as model system for the bioreceptor-analyte couple, due to their extremely high affinity. By simple addition of ZnO NPs to SA aqueous solution, spin-coated ZnO-modified bio-interlayer could be prepared for further assembly of the final OFET biosensor. Both the electrical characteristics and the biotin sensing were performed systematically comparing bare and ZnO-bearing FBI-OFET biosensors. The presence of ZnO NPs allowed preserving the field-effect and the pM limit of detections towards biotin for over 1 year. The bare device, on the contrary, turned after few weeks into a resistive behavior and the SA protein was de-activated, probably due to poly(3-hexylthiophene) (P3HT) degradation. The rationalization of these findings was assessed by means of X-ray photoelectron spectroscopy (XPS) characterization of P3HT/SA-ZnO NPs and P3HT/SA FBIs, freshly prepared and after ageing, indicating the central role of zinc oxide in the device improved performance level.

2. Experimental

2.1 Synthesis of ZnO Nanoparticles

An electrochemical-thermal method was used to prepare ZnO NPs following a previously reported procedure [31]. A three-electrode cell was employed, consisting of two zinc sheets (2x1 cm^2, 1 mm thick, 99.99+%, Goodfellow Ltd) as working and counter electrodes, and an Ag/AgCl (in saturated KCl) reference electrode. Zinc electrodes were polished using sandpaper and Al_2O_3 powder (purum p.a., 99.7%, Fluka), followed by ultrasonication in Milli-Q water for 15 min. The electrodes were then activated in 1 M HCl (ACS reagent, 37%, Sigma Aldrich) for 30 s. The synthesized nanoparticles mass was estimated by difference of zinc sheets weights, before and after the process. The electrosynthesis was carried out galvanostatically (j = 10 mA/cm^2) for 1 h, under vigorous stirring at room temperature, with a CH-1140b potentiostat-galvanostat (CH Instruments, USA). The electrolytic medium was composed of 1 g/L poly(sodium 4-styrenesulfonate) (PSS, average Mw ~ 70,000, powder, Sigma Aldrich), dissolved in 30 mM $NaHCO_3$ (purum p.a., ≥ 99.0%, Fluka) aerated aqueous solution. After the electrochemical step, the colloidal dispersion was centrifuged at 5000 rpm for 45 minutes. The resulting precipitate was dried overnight at 70°C, and then calcined at 600°C for 1 h.

2.2 Fabrication of FBI-OFET devices

SA and SA-ZnO NPs FBI-OFETs were prepared by a two-step spin-coating procedure. 50 μL of 50 μg/mL SA (Sigma Aldrich) aqueous solution (LC-MS grade water, Sigma) or of SA (50 μg/mL) + ZnO NPs (0.5 g/L) mixed suspension were deposited onto SiO_2/Si clean substrates. p-doped Si/SiO_2 (Si:B, oxide: 300 nm, <110>) wafers were purchased from Si-Mat Silicon Material. Spin coating was carried out at 200 rpm for 60 min allowing slow formation of a thin-film. Afterwards, the deposition of the OSC layer was performed by spinning a 2.6 g/L chloroform (puriss. > 99.8%, ACS reagent) solution of poly(3-hexylthiophene-2,5-diyl) (P3HT, regioregular, electronic grade, 99.995% trace metal basis, Mw ~ 15.000 – 45.000, Rieke® Metals Inc.) [35–37] at 2000 rpm for 1 min. A Laurell Technology Corporation spin coater (model WS – 650 MZ – NPP/LITE) was employed throughout the process. Source (S) and drain (D) gold contacts were deposited by thermal evaporation (8×10^{-7} torr) from high-purity pellets (99.99%, Gambetti Kenologia) through a shadow mask. The length (L) and the width (W) of the resulting channel are 0.2 mm and 4 mm, respectively. The gate contact (G) was obtained by scratching SiO_2 layer with a diamond tip in order to reach the highly doped Si surface underneath. To minimize leakage currents, the P3HT film was patterned around the source and drain electrodes. Different layers (and corresponding FBI-OFETs) were labeled as P3HT/SA and P3HT/SA-ZnO NPs. When not in use, the devices were stored in the dark in a standard bench-top desiccator (Kartell) with polycarbonate lid, polypropylene base and desiccant tray. Silica gel with indicator (Sigma Aldrich) was used as desiccant with a humidity level around 40%.

2.3 FBI-OFETs electrical characterization and sensing measurements

Electrical measurements were carried out using a Keithley Model 4200-SCS semiconductor analyser. The OFETs were characterized by measuring the I_{DS}-V_{DS} output characteristics, where the drain to source current (I_{DS}) is recorded at different gate voltages (V_G) ranging from -20 to -100 V with a step of 20 V, while the source and drain bias (V_{DS}) is swept from 0 to -100 V. For the transfer characteristics, the I_{DS} was measured at different gate voltages and at constant V_{DS}= -80 V. The gate voltage was cycled from the OFF to the ON state and backwards using pulses of alternating polarities (AP sweep mode). The gate voltage pulses were generated by selecting the voltage list sweep option, in the software provided by Keithley, and setting the pulse amplitude to gradually increase from 0 to -100 V with a step of 4 V and backwards, while alternating the polarity at each step. In this way, as it has been previously shown, hysteretic phenomena due to bias stressing are significantly suppressed [38]. Electrical parameters (μ_{FET} and V_T) were extracted from the I_{DS}-V_{GS} transfer characteristics in the saturation regime according to a well-known procedure [39]. The I_{on}/I_{off} was determined by taking the value of I_{on} at $V_{DS} = V_G$ = max and I_{off} at V_{DS} = max and V_G = 0 V. For the sensing measurements, the OFET channel is initially exposed to 0.5 μL of water and then to increasing concentrations of biotin aqueous solutions ranging from 0.01 to 100 ppb. At each exposure, the device is incubated for 10 min, and then it is rinsed with water three times to remove the unreacted biotin. Finally, the channel is dried under

nitrogen flow for another 10 min and the transfer I–V characteristic curve is measured in dry state under N_2 flow. The porous morphology of the P3HT allows biotin molecules to efficiently diffuse through the P3HT layer and reach the proteins deposited underneath [40,41]. The response to water drop is first registered and taken as baseline. Fractional current response is evaluated as $\Delta I/I_0 = (I-I_0)/I_0$ limiting the effect of inter-device variability, where $\Delta I = I_{biot} - I_0$, I_{biot} is the current after exposure to different concentrations of biotin and I_0 the current after water exposure (baseline). Signal (I) and baseline (I_0) values are taken at V_{GS} = -100 V and at V_{DS} = -80 V from the transfer characteristics.

P3HT/ZnO NPs devices, not implementing the protein (SA), were also prepared and tested in control experiments.

2.4 XPS characterization of active layers

All the prepared layers were investigated by X-ray Photoelectron Spectroscopy (XPS). A PHI Versaprobe II spectrometer equipped with monochromatized Al Kα radiation (1486.6 eV) was used. Survey spectra were acquired with a pass energy of 117.4 eV and an energy step of 1.0 eV; whereas high-resolution (HR) spectra were acquired with a pass energy of 58.7 eV and an energy step of 0.125 eV. C1s, O1s, Si2p, S2p, N1s, Zn2p, $ZnL_3M_{45}M_{45}$ regions were analyzed. Additional sputtering depth profile was carried out on P3HT/SA-ZnO NPs hybrid layers. Ar^+ sputtering was performed on a 2x2-mm^2 area setting the acceleration voltage at 1 kV and current at 1

μA. The elemental composition analysis was performed with MultiPack™ (v. 9.5.0, PHI-ULVAC). Peak fitting procedures were performed using the software CasaXPS™ (v. 2.3.18). Binding energy (BE) scale was corrected taking as reference C1s component at 284.8 eV. P3HT, P3HT/ZnO NPs, P3HT/SA, P3HT/SA-ZnO NPs, and SA-ZnO NPs were investigated, either fresh and after ageing.

3. Results and discussion

The electrical properties of the P3HT/SA-ZnO NPs FBI-OFETs devices were evaluated and compared with those of the bare P3HT/SA ones. A general scheme of P3HT/SA-ZnO NPs structure is presented in Figure 1. Source and drain gold contacts are deposited by thermal evaporation on the organic semiconductor (P3HT) film, which is directly spin-coated on the protein/ZnO NPs mixed layer; the latter is deposited directly on the SiO_2 surface.

Figure 2 shows the output I-V curves for bare P3HT/SA and of the P3HT/SA-ZnO NPs devices along with the transfer characteristics in semi logarithmic scale of the drain current I_{DS} and the gate leakage I_{GS} *versus* the gate voltage V_G. The output characteristics of the FBI-OFET bioelectronic device exhibit current modulation with well-shaped linear and saturated regions as well as negligible hysteresis and low leakage current. An enhancement of the device performance is readily observed in the presence of the ZnO NPs in the SA inter-biolayer laying between the semiconductor and silicon dioxide. More specifically, the field-effect mobility (μ_{FET}) increases of about one order

of magnitude, the threshold voltage (V_T) shifts to higher positive values and the $I_{on/off}$ ratio is improved also by at least one order of magnitude, when ZnO NPs are integrated in the device. This trend is in agreement with the behavior previously observed on P3HT-based OTFT bearing a ZnO NPs interlayer [31].

To investigate the effect of ZnO NPs in the sensing performance, the P3HT/SA-ZnO NPs FBI-OFETs were exposed to increasing concentrations of biotin. Streptavidin-biotin couple is known to form one of the strongest non-covalent bond in biological systems, thus being a gold standard for studying protein/ligand interactions [42]. As a result, this binary system has often been used to probe the analytical performance of several biosensing platforms [43,44]. In this work, streptavidin and biotin are proposed as capturing protein and target molecule (analyte), respectively. While the layer-by-layer approach has been demonstrated to form controlled films [10,40,41] resulting in rather sensitive devices [10], the spin-coating technique provides a valid alternative for scalable processes and uncharged molecules. As a result, we compared the sensing performance of spin deposited P3HT/SA and P3HT/SA-ZnO NPs biosensors.

Typical curves for P3HT/SA-ZnO NPs device after exposure to biotin solutions are given in Figure 3a. A gradual current decrease can be observed in correlation with the exposure of the device to increasing biotin concentration. In Figure 3b the plot of $-\Delta I/I_0$ *vs.* the analyte concentration is presented for both P3HT/SA and P3HT/SA-ZnO NPs FBI-OFET biosensors. In a previous work [7], it was shown that SA-biotin complex reached saturation after 25 min incubation. Additionally, employing a saturated system

as FBI it was demonstrated that no response to biotin was measured anymore. Moreover, 10 min was proven to be sufficient to achieve the binding without losing sensitivity to biotin [45]. Similar current fractional changes were obtained on P3HT/SA devices working at 15 min-incubation time [7,10], indicating that this parameter is not critical in the adopted sensing protocol. As a control experiment, a calibration curve measured on a P3HT/ZnO NPs device not comprising the SA layer is also shown in Figure 3b (black hollow circles), demonstrating that the sensing is only enabled when the SA is present. Figures 3c and 3d show the variation of field-effect mobility and the threshold voltage, extracted as reported in [39], after exposure to biotin. As it is apparent, the measured current fractional changes are mostly ascribable to mobility variations. This occurrence has been already addressed as caused by the disorder induced, locally, by the proteins structural and/or conformational changes upon ligand binding that impact on the OSC transport properties. No significant change in V_T is seen because the reorientation of the SA permanent dipole moment is impaired when the protein is blocked underneath the OSC [45].

The rather invariant slope of the calibration curves shown in Figure 3b reveals that the analytical sensitivity of the FBI-OFET sensor does not appreciably change upon integration of the ZnO NPs. This occurrence suggests that, expectedly, the NPs do not enhance the density of capturing molecules active binding sites nor they deactivate the protein bio-activity. On the other hand, rather surprisingly, when the P3HT/SA-ZnO

NPs FBI-OFET device was tested two months after its fabrication against biotin, the response was very much alike to the pristine (fresh) one. More importantly, after storing a device for 1 year in a standard bench-top desiccator, it showed still very good electrical performances and the detection of biotin was still possible, implying that the presence of ZnO NPs can significantly improve the stability in ambient air of FET devices endowed with an organic channel material. By contrast, the electrical performance of the P3HT/SA devices was barely stable already after 2 month-storage in the same conditions. The current-voltage profile of the output characteristic curve (Figure S1, Supporting Information) showed an increase of the off-state conduction and a more resistor –like behavior of the I_{DS} to the V_{DS} sweep. Moreover, the I_{DS} current saturation was hardly achieved. Therefore, the device was not employed further for carrying out sensing measurements.

The electrical performance of the P3HT/ZnO NPs and a bare P3HT based OFETs after different storage intervals is shown in Figure 4 and additional results are presented in Figure S2 (Supporting Information). The devices were kept for 4 months, measuring their electrical responses at given time intervals. When not in use, the devices were kept in a desiccator and in the dark.

It is worth noticing that in the absence of the inorganic ZnO NPs interlayer, the transistor is unstable and loses completely the initial performance level after 120 days. On the other hand, the P3HT degradation is strongly attenuated when the ZnO NPs are

incorporated in the device structure. Increment on V_T and reduction of μ_{FET} and I_{on}/I_{off} are found for the P3HT devices (Figure S2, Supporting Information), a typical trend observed when a p-type OSC is exposed to water/humidity [12]. By contrast, such detrimental effect was less evident on ZnO NP-modified OFETs, whose mobility was even increased with time.

The impact of ZnO NPs on the stability of the OSC was investigated by means of X-Ray Photoelectron Spectroscopy (XPS). To this aim, the characteristic photoelectron signals for P3HT, namely C1s and S2p regions were analyzed. It is received that moisture and oxygen are responsible for reduced performance of OSCs [12,46]. When the degradation occurs, the C1s signal shows an increase in oxygenated components (*e.g.* at binding energy, BE above 287 eV). In this respect interesting is the study of Hoshino *et al.* that investigated the influence of moisture and oxygen in P3HT-based FETs [46]. It was shown that the device operation was more assailable to changes in the presence of atmospheric moisture than absolute O_2 in ambient pressure. The influence of moisture dominated the device performance much more rapidly than the doping effect of O_2. Hence, P3HT and P3HT/SA layers modified with ZnO NPs, were investigated by XPS considering 1-year ageing time. First, surface chemical composition was studied and typical results are reported in Table S1 (Supporting Information). Here, no significant difference in terms of composition between aged and fresh samples can be seen. Depth profile analysis was also carried out on P3HT/SA-

ZnO NPs samples and the results in terms of El% normalized to Si% (attributed only to the substrate) are presented in Fig. S3. Data show that ZnO NPs are embedded below a very thin P3HT layer and that the inorganic semiconductor is homogeneously distributed in the inner part of the device active layer. XPS depth profiling is discussed in more detail in the supplementary information. The C1s and S2p photoelectron signals relevant to 1-year aged P3HT and P3HT/SA-ZnO NPs are presented in Figure 5. It is evident that both XP regions are rather similar in the two samples. Based on the C1s signal, however it seems that the presence of ZnO NPs only marginally preserves the OSC from oxidative degradation. Moreover, Sulphur shows the typical doublet of thiophene rings ($S2p_{3/2}$ main component at BE = 163.7 ± 0.2 eV) [41] without any evidence of oxidation (no additional components above 167 eV) [47].

More interesting information could be derived from the XPS analysis of the Zn speciation on fresh and aged devices. Zinc(II) species can be discriminated by means of $ZnL_3M_{45}M_{45}$ Auger signal (expressed in kinetic energy, KE) and of the modified Auger parameter α' [31,48–50], where α' is calculated as $BE(Zn2p_{3/2}) + KE(ZnL_3M_{45}M_{45})$. Indeed, $Zn2p_{3/2}$ signal in fresh pristine (BE= 1022.8 ± 0.1 eV) and aged P3HT/SA-ZnO NPs (BE= 1022.6 ± 0.1 eV) samples. Typical $ZnL_3M_{45}M_{45}$ regions relevant to fresh and 1-year aged P3HT/SA-ZnO NPs samples are shown in Figure 6. The position for $ZnL_3M_{45}M_{45}$ maximum is found at KE= 987.1 ± 0.1 eV for fresh samples, whereas it falls at KE= 986.6 ± 0.1 eV after ageing. By calculating α', it can be observed that the

values for fresh *vs.* aged hybrid layers are significantly different (2009.9 ± 0.2 eV vs. 2009.2 ± 0.2 eV). In particular, the former is in agreement with the presence of zinc oxide , the latter is compatible with the formation of zinc hydroxide [49]. Such shift cannot be explained by invoking a stabilizing effect due to protein-Zn complexation. In fact, typical α' values reported for zinc complexes with amino acid-like derivatives and porphyrins are equal or above 2010 eV [51–53]. P3HT/ZnO NPs samples (not bearing streptavidin) were characterized to corroborate this finding, both just after their preparation and after ageing. $ZnL_3M_{45}M_{45}$ regions relevant to fresh (panel a) and 1-year aged (panel b) P3HT/ZnO NPs films were acquired and fitted providing similar results (Figure S4, Supporting information). In fact, the signal position shifted at lower KE in aged samples, as already found on P3HT/SA-ZnO NPs (Fig. 6). Considering XPS surface sensitivity, this is an indirect evidence that ZnO NPs undergo a process of surface hydration behaving as a sort of hygroscopic "capturing layer" for humidity, hence keeping the P3HT interfaces more free from such a degradation agent. This means that the degradation of P3HT as well as that of the bioreceptor are limited by the presence of this additional component, and this fortunate occurrence preserves the sensing properties of the whole FBI-OFET device for one full year enabling also much better electronic performances as both the field-effect mobility and the on-off ratio are enhanced by at least one order of magnitude.

4. Conclusions

FBI-OFET biosensors integrating ZnO NPs were easily prepared by a fast and low-cost procedure. It was shown that ZnO NPs improved the overall device electrical performances by at least one order of magnitude without altering the sensing figures of merit. Moreover, the ZnO NPs endowed the FBI-OFET biosensor with an exceptionally prolonged shelf-lifetime. Response to biotin in the low pM range of concentrations was obtained even by using 1-year aged devices. The role of ZnO NPs in the observed phenomenon was investigated by testing OFET devices to quantify the effective influence of the nanomaterial towards the OSC stabilization. The mechanism of the improved stability was discussed in terms of ZnO NP surface hydration upon time based on XPS results. Our results show that n-type ZnO NPs dispersed into p-type polymers are a promising material for efficient and stable electronic biosensors. The interaction of ZnO with polymers may provide ways of obtaining unique or enhanced electronic properties in OFETs too.

Acknowledgements

R.A.P. and K.M. acknowledge the financial support of Fondo di Sviluppo e Coesione 2007-2013 – APQ Ricerca Regione Puglia "Programma regionale a sostegno della specializzazione intelligente e della sostenibilità sociale ed ambientale - FutureInResearch" projects B164PG8 and ML5BJ85.

References

[1] C. Liao, M. Zhang, M.Y. Yao, T. Hua, L. Li, F. Yan, Flexible Organic Electronics in Biology: Materials and Devices, Adv. Mater. 27 (2015) 7493–7527. doi:10.1002/adma.201402625.

[2] F. Marinelli, A. Dell'Aquila, L. Torsi, J. Tey, G.P. Suranna, P. Mastrorilli, G. Romanazzi, C.F. Nobile, S.G. Mhaisalkar, N. Cioffi, F. Palmisano, An organic field effect transistor as a selective NOx sensor operated at room temperature, Sens. Actuators B Chem. 140 (2009) 445–450. doi:10.1016/j.snb.2009.04.035.

[3] L. Torsi, F. Marinelli, M.D. Angione, A. Dell'Aquila, N. Cioffi, E.D. Giglio, L. Sabbatini, Contact effects in organic thin-film transistor sensors, Org. Electron. 10 (2009) 233–239. doi:10.1016/j.orgel.2008.11.009.

[4] L. Torsi, M. Magliulo, K. Manoli, G. Palazzo, Organic field-effect transistor sensors: a tutorial review, Chem. Soc. Rev. 42 (2013) 8612–8628. doi:10.1039/C3CS60127G.

[5] M. Magliulo, K. Manoli, E. Macchia, G. Palazzo, L. Torsi, Tailoring Functional Interlayers in Organic Field-Effect Transistor Biosensors, Adv. Mater. (2014). doi:10.1002/adma.201403477.

[6] W.-H. Zhang, B.-J. Jiang, P. Yang, Proteins as functional interlayer in organic field-effect transistor, Chin. Chem. Lett. 27 (2016) 1339–1344. doi:10.1016/j.cclet.2016.06.044.

[7] M.D. Angione, S. Cotrone, M. Magliulo, A. Mallardi, D. Altamura, C. Giannini, N. Cioffi, L. Sabbatini, E. Fratini, P. Baglioni, G. Scamarcio, G. Palazzo, L. Torsi, Interfacial electronic effects in functional biolayers integrated into organic field-effect transistors, Proc. Natl. Acad. Sci. (2012). doi:10.1073/pnas.1200549109.

[8] G. Palazzo, M. Magliulo, A. Mallardi, M.D. Angione, D. Gobeljic, G. Scamarcio, E. Fratini, F. Ridi, L. Torsi, Electronic transduction of proton translocations in nanoassembled lamellae of bacteriorhodopsin, ACS Nano. 8 (2014) 7834–7845. doi:10.1021/nn503135y.

[9] W. Shi, X. Yu, Y. Zheng, J. Yu, DNA based chemical sensor for the detection of nitrogen dioxide enabled by organic field-effect transistor, Sens. Actuators B Chem. 222 (2016) 1003–1011. doi:10.1016/j.snb.2015.09.040.

[10] M. Magliulo, A. Mallardi, R. Gristina, F. Ridi, L. Sabbatini, N. Cioffi, G. Palazzo, L. Torsi, Part per Trillion Label-Free Electronic Bioanalytical Detection, Anal. Chem. 85 (2013) 3849–3857. doi:10.1021/ac302702n.

[11] M. Nikolka, I. Nasrallah, B. Rose, M.K. Ravva, K. Broch, A. Sadhanala, D. Harkin, J. Charmet, M. Hurhangee, A. Brown, S. Illig, P. Too, J. Jongman, I. McCulloch, J.-L. Bredas, H. Sirringhaus, High operational and environmental stability of high-mobility conjugated polymer field-effect transistors through the use of molecular additives, Nat. Mater. 16 (2016) 356.

[12] E.K. Lee, M.Y. Lee, C.H. Park, H.R. Lee, J.H. Oh, Toward Environmentally Robust Organic Electronics: Approaches and Applications, Adv. Mater. (2017) 1703638–n/a. doi:10.1002/adma.201703638.

[13] D. Yu, Y.-Q. Yang, Z. Chen, Y. Tao, Y.-F. Liu, Recent progress on thin-film encapsulation technologies for organic electronic devices, Opt. Commun. 362 (2016) 43–49. doi:10.1016/j.optcom.2015.08.021.

[14] L.A. Majewski, J.W. Kingsley, C. Balocco, A.M. Song, Influence of processing conditions on the stability of poly(3-hexylthiophene)-based field-effect transistors, Appl. Phys. Lett. 88 (2006) 222108. doi:10.1063/1.2208938.

[15] O. Knopfmacher, M.L. Hammock, A.L. Appleton, G. Schwartz, J. Mei, T. Lei, J. Pei, Z. Bao, Highly stable organic polymer field-effect transistor sensor for selective detection in the marine environment, Nat. Commun. 5 (2014) 2954.

[16] H.O. Seo, M.-G. Jeong, K.-D. Kim, D.H. Kim, Y.D. Kim, D.C. Lim, Studies of degradation behaviors of poly (3-hexylthiophene) layers by X-ray photoelectron spectroscopy, Surf. Interface Anal. 46 (2014) 544–549. doi:10.1002/sia.5557.

[17] X. Jia, S. Dong, E. Wang, Engineering the bioelectrochemical interface using functional nanomaterials and microchip technique toward sensitive and portable electrochemical biosensors, Biosens. Bioelectron. 76 (2016) 80–90. doi:10.1016/j.bios.2015.05.037.

[18] M.D. Angione, R. Pilolli, S. Cotrone, M. Magliulo, A. Mallardi, G. Palazzo, L. Sabbatini, D. Fine, A. Dodabalapur, N. Cioffi, L. Torsi, Carbon based materials for electronic bio-sensing, Mater. Today. 14 (2011) 424–433. doi:10.1016/S1369-7021(11)70187-0.

[19] J. Chen, S.M. Andler, J.M. Goddard, S.R. Nugen, V.M. Rotello, Integrating recognition elements with nanomaterials for bacteria sensing, Chem. Soc. Rev. 46 (2017) 1272–1283. doi:10.1039/C6CS00313C.

[20] A.F.S. Abu-Hani, F. Awwad, Y.E. Greish, A.I. Ayesh, S.T. Mahmoud, Design, fabrication, and characterization of low-power gas sensors based on organic-inorganic nano-composite, Org. Electron. 42 (2017) 284–292. doi:10.1016/j.orgel.2016.12.050.

[21] L. Xue, W. Wang, Y. Guo, G. Liu, P. Wan, Flexible polyaniline/carbon nanotube nanocomposite film-based electronic gas sensors, Sens. Actuators B Chem. 244 (2017) 47–53. doi:10.1016/j.snb.2016.12.064.

[22] J.W. Park, C. Lee, J. Jang, High-performance field-effect transistor-type glucose biosensor based on nanohybrids of carboxylated polypyrrole nanotube wrapped graphene sheet transducer, Sens. Actuators B Chem. 208 (2015) 532–537. doi:10.1016/j.snb.2014.11.085.

[23] S.K. Arya, S. Saha, J.E. Ramirez-Vick, V. Gupta, S. Bhansali, S.P. Singh, Recent advances in ZnO nanostructures and thin films for biosensor applications: Review, Anal. Chim. Acta. 737 (2012) 1–21. doi:10.1016/j.aca.2012.05.048.

[24] S.S. Bhat, A. Qurashi, F.A. Khanday, ZnO nanostructures based biosensors for cancer and infectious disease applications: Perspectives, prospects and promises, TrAC Trends Anal. Chem. 86 (2017) 1–13. doi:10.1016/j.trac.2016.10.001.

[25] B.N. Pal, P. Trottman, J. Sun, H.E. Katz, Solution-Deposited Zinc Oxide and Zinc Oxide/Pentacene Bilayer Transistors: High Mobility n-Channel, Ambipolar, and Nonvolatile Devices, Adv. Funct. Mater. 18 (2008) 1832–1839. doi:10.1002/adfm.200701430.

[26] H. Tai, X. Li, Y. Jiang, G. Xie, X. Du, The Enhanced Formaldehyde-Sensing Properties of P3HT-ZnO Hybrid Thin Film OTFT Sensor and Further Insight into Its Stability, Sensors. 15 (2015) 2086–2103. doi:10.3390/s150102086.

[27] A. Choi, K. Kim, H.-I. Jung, S.Y. Lee, ZnO nanowire biosensors for detection of biomolecular interactions in enhancement mode, Sens. Actuators B Chem. 148 (2010) 577–582. doi:10.1016/j.snb.2010.04.049.

[28] M.F.M. Fathil, M.K. Md Arshad, A.R. Ruslinda, S.C.B. Gopinath, M. Nuzaihan M.N., R. Adzhri, U. Hashim, H.Y. Lam, Substrate-gate coupling in ZnO-FET biosensor for cardiac troponin I detection, Sens. Actuators B Chem. 242 (2017) 1142–1154. doi:10.1016/j.snb.2016.09.131.

[29] A.N. Aleshin, I.P. Shcherbakov, A light-emitting field-effect transistor based on a polyfluorene–ZnO nanoparticles film, J. Phys. Appl. Phys. 43 (2010) 315104. doi:10.1088/0022-3727/43/31/315104.

[30] Y. Zhou, S.-T. Han, L. Zhou, Y. Yan, L.-B. Huang, J. Huang, V.A.L. Roy, Flexible organic/inorganic heterojunction transistors with low operating voltage, J. Mater. Chem. C. 1 (2013) 7073–7080. doi:10.1039/C3TC31456A.

[31] R.A. Picca, M.C. Sportelli, D. Hötger, K. Manoli, C. Kranz, B. Mizaikoff, L. Torsi, N. Cioffi, Electrosynthesis and characterization of ZnO nanoparticles as inorganic component in organic thin-film transistor active layers, Electrochimica Acta. 178 (2015) 45–54. doi:10.1016/j.electacta.2015.07.122.

[32] A.K. Diallo, M. Gaceur, N. Berton, O. Margeat, J. Ackermann, C. Videlot-Ackermann, Towards solution-processed ambipolar hybrid thin-film transistors based on ZnO nanoparticles and P3HT polymer, Superlattices Microstruct. 58 (2013) 144–153. doi:10.1016/j.spmi.2013.03.012.

[33] R. Ahmad, N. Tripathy, Y.-B. Hahn, High-performance cholesterol sensor based on the solution-gated field effect transistor fabricated with ZnO nanorods, Biosens. Bioelectron. 45 (2013) 281–286. doi:10.1016/j.bios.2013.01.021.

[34] X. Liu, P. Lin, X. Yan, Z. Kang, Y. Zhao, Y. Lei, C. Li, H. Du, Y. Zhang, Enzyme-coated single ZnO nanowire FET biosensor for detection of uric acid, Sens. Actuators B Chem. 176 (2013) 22–27. doi:10.1016/j.snb.2012.08.043.

[35] A.J. Lovinger, D.D. Davis, R. Ruel, L. Torsi, A. Dodabalapur, H.E. Katz, Morphology of α-hexathienyl thin-film-transistor films, J. Mater. Res. 10 (1995) 2958–2962. doi:10.1557/JMR.1995.2958.

[36] L. Torsi, A. Dodabalapur, A.J. Lovinger, H.E. Katz, R. Ruel, D.D. Davis, K.W. Baldwin, Rapid thermal processing of .alpha.-hexathienylene thin-film transistors, Chem. Mater. 7 (1995) 2247–2251. doi:10.1021/cm00060a010.

[37] A.J. Lovinger, D.D. Davis, A. Dodabalapur, H.E. Katz, L. Torsi, Single-Crystal and Polycrystalline Morphology of the Thiophene-Based Semiconductor α-Hexathienyl (α-6T), Macromolecules. 29 (1996) 4952–4957. doi:10.1021/ma960111b.

[38] K. Manoli, M.M. Patrikoussakis, M. Magliulo, L.M. Dumitru, M.Y. Mulla, L. Sabbatini, L. Torsi, Pulsed voltage driven organic field-effect transistors for high stability transient current measurements, Org. Electron. 15 (2014) 2372–2380. doi:10.1016/j.orgel.2014.06.034.

[39] L. Torsi, A. Dodabalapur, Organic Thin-Film Transistors as Plastic Analytical Sensors, Anal. Chem. 77 (2005) 380 A-387 A. doi:10.1021/ac053475n.

[40] M. Magliulo, D. Altamura, C. Di Franco, M.V. Santacroce, K. Manoli, A. Mallardi, G. Palazzo, G. Scamarcio, C. Giannini, L. Torsi, Structural and Morphological Study of a Poly(3-hexylthiophene)/Streptavidin Multilayer Structure Serving as Active Layer in Ultra-Sensitive OFET Biosensors, J. Phys. Chem. C. 118 (2014) 15853–15862. doi:10.1021/jp504652u.

[41] M.C. Sportelli, R.A. Picca, K. Manoli, M. Re, E. Pesce, L. Tapfer, C. Di Franco, N. Cioffi, L. Torsi, Surface analytical characterization of Streptavidin/poly(3–hexylthiophene) bilayers for bio-electronic applications, Appl. Surf. Sci. 420 (2017) 313–322. doi:10.1016/j.apsusc.2017.05.086.

[42] M. González, L.A. Bagatolli, I. Echabe, J.L.R. Arrondo, C.E. Argaraña, C.R. Cantor, G.D. Fidelio, Interaction of Biotin with Streptavidin: THERMOSTABILITY AND CONFORMATIONAL CHANGES UPON BINDING, J. Biol. Chem. 272 (1997) 11288–11294. doi:10.1074/jbc.272.17.11288.

[43] D. Sarkar, W. Liu, X. Xie, A.C. Anselmo, S. Mitragotri, K. Banerjee, MoS2 Field-Effect Transistor for Next-Generation Label-Free Biosensors, ACS Nano. 8 (2014) 3992–4003. doi:10.1021/nn5009148.

[44] A.V. Kabashin, P. Evans, S. Pastkovsky, W. Hendren, G.A. Wurtz, R. Atkinson, R. Pollard, V.A. Podolskiy, A.V. Zayats, Plasmonic nanorod metamaterials for biosensing, Nat Mater. 8 (2009) 867–871. doi:10.1038/nmat2546.

[45] E. Macchia, D. Alberga, K. Manoli, G.F. Mangiatordi, M. Magliulo, G. Palazzo, F. Giordano, G. Lattanzi, L. Torsi, Organic bioelectronics probing conformational changes in surface confined proteins, Sci. Rep. 6 (2016). doi:10.1038/srep28085.

[46] S. Hoshino, M. Yoshida, S. Uemura, T. Kodzasa, N. Takada, T. Kamata, K. Yase, Influence of moisture on device characteristics of polythiophene-based field-effect transistors, J. Appl. Phys. 95 (2004) 5088–5093. doi:10.1063/1.1691190.

[47] National Institute of Standards and Technology, XPS Database, NIST X-Ray Photoelectron Spectrosc. Database Version 41. (2012). http://srdata.nist.gov/xps.

[48] C.D. Wagner, L.H. Gale, R.H. Raymond, Two-dimensional chemical state plots: a standardized data set for use in identifying chemical states by x-ray photoelectron spectroscopy, Anal. Chem. 51 (1979) 466–482. doi:10.1021/ac50040a005.

[49] L.S. Dake, D.R. Baer, J.M. Zachara, Auger parameter measurements of zinc compounds relevant to zinc transport in the environment, Surf. Interface Anal. 14 (1989) 71–75. doi:10.1002/sia.740140115.

[50] R.A. Picca, M.C. Sportelli, R. Lopetuso, N. Cioffi, Electrosynthesis of ZnO nanomaterials in aqueous medium with CTAB cationic stabilizer, J. Sol-Gel Sci. Technol. 81 (2017) 338–345. doi:10.1007/s10971-016-4268-9.

[51] D. Atzei, D. De Filippo, A. Rossi, A. Lai, G. Saba, R. Bucci, IR, NMR, XPS study of 1-(d-3-mercapto-2-methylpropionyl)-l-proline and its zinc complexes, Spectrochim. Acta Part Mol. Spectrosc. 48 (1992) 911–919. doi:10.1016/0584-8539(92)80167-U.

[52] D. Atzei, D. De Filippo, A. Rossi, R. Caminiti, C. Sadun, XPS and LAXS study of 1,3-thiazolidine-2-thione and its complexes with Co(II) and Zn(II), Spectrochim. Acta. A. Mol. Biomol. Spectrosc. 51 (1995) 11–20. doi:10.1016/0584-8539(94)E0083-M.

[53] J. Spadavecchia, C. Méthivier, J. Landoulsi, C.-M. Pradier, Interaction of ZnII Porphyrin with TiO2 Nanoparticles: From Mechanism to Synthesis of Hybrid Nanomaterials, ChemPhysChem. 14 (2013) 2462–2469. doi:10.1002/cphc.201300193.

Captions to Figures

Figure 1. Schematic illustration of the P3HT/SA-ZnO NPs FBI-OFET device structure.

Figure 2. I_{DS}-V_{DS} output characteristics for the P3HT/SA (a) and the P3HT/SA-ZnO NPs (b) FBI-OFETs. Panel (c) shows the I_{DS}-V_G transfer characteristics for bare P3HT/SA (black) and P3HT/SA-ZnO NPs (red) devices (V_{DS} = -80 V) along with the I_G leakage currents (dotted lines).

Figure 3. (a) I_{DS}-V_{GS} transfer characteristics at V_{DS} = −80 V for the P3HT/SA-ZnO NPs FBI-OFET exposed to water and different biotin concentrations; relative current response of fresh and aged P3HT/SA-ZnO NPs, fresh P3HT/SA, fresh P3HT/ZnO NPs OFETs to different biotin concentrations on a semi-logarithmic scale (b); relative change of the field-effect mobility (c) and threshold voltage (d). Each data point is the mean value over three replicates measured on different devices and error bars are taken as one standard deviation.

Figure 4. I_{DS}-V_{DS} output characteristics with V_G ranging from 20 V to -100 V for P3HT/ZnO NPs (a) and bare P3HT (b), fresh and after 120 days storage OFETs. The I_{DS}-V_G transfer curves are presented at different storage times for P3HT/ZnO NPs (c) and (d) bare P3HT devices.

Figure 5. C1s (a) and S2p (b) XP regions for aged samples: bare P3HT (solid curves) and P3HT/SA-ZnO NPs (dashed curves).

Figure 6. $ZnL_3M_{45}M_{45}$ regions relevant to fresh (a) and aged (b) P3HT/SA-ZnO NPs.

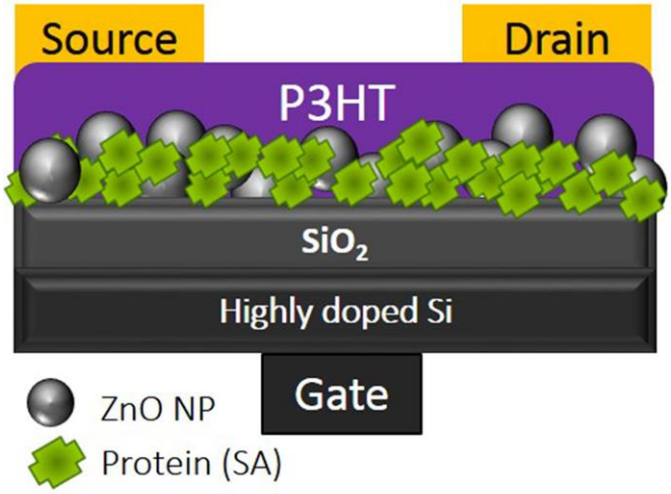
Source
Drain
P3HT
SiO2
Highly doped Si
Gate
ZnO NP
Protein (SA)

Fig. 1

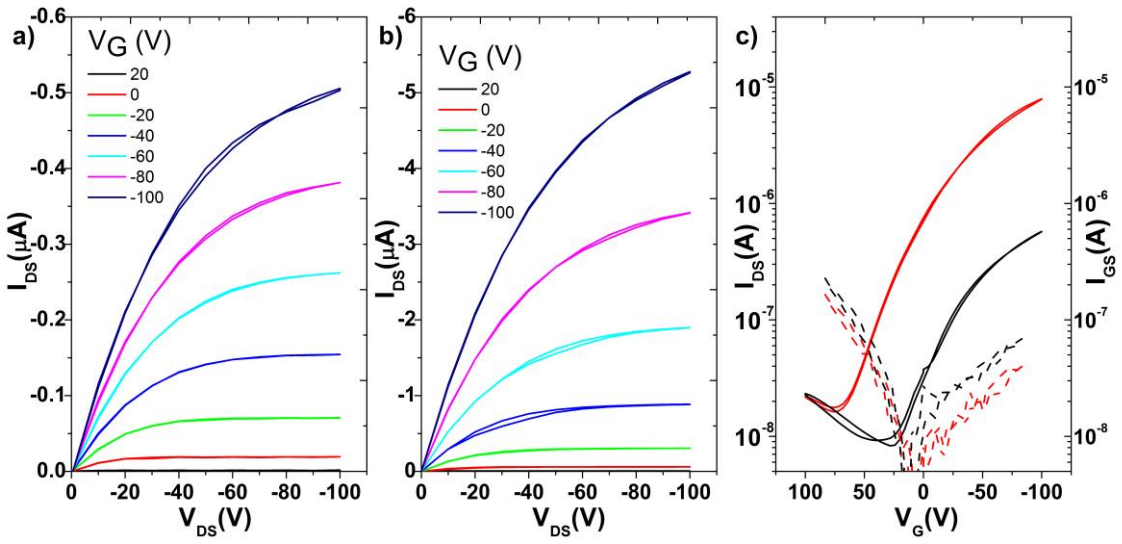
a)
b)
c)
VG (V)
20
0
-20
-40
-60
-80
-100
IDS(μA)
VDS(V)
IDS(A)
IGS(A)
VG(V)

Fig. 2

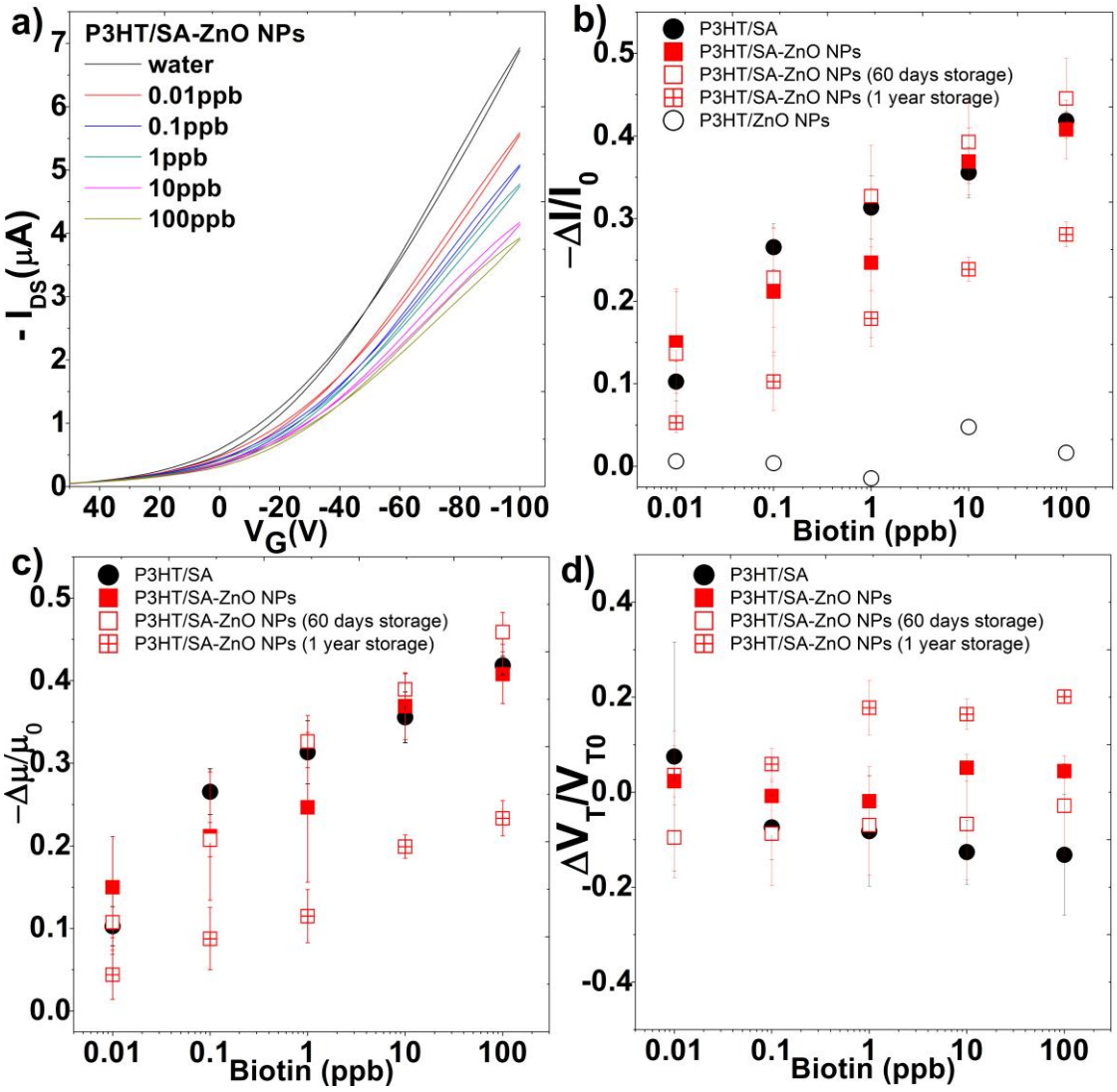
a)
P3HT/SA-ZnO NPs
water
0.01ppb
0.1ppb
1ppb
10ppb
100ppb
- I_DS(μA)
V_G(V)
b)
P3HT/SA
P3HT/SA-ZnO NPs
P3HT/SA-ZnO NPs (60 days storage)
P3HT/SA-ZnO NPs (1 year storage)
P3HT/ZnO NPs
−ΔI/I_0
Biotin (ppb)
c)
P3HT/SA
P3HT/SA-ZnO NPs
P3HT/SA-ZnO NPs (60 days storage)
P3HT/SA-ZnO NPs (1 year storage)
−Δμ/μ_0
Biotin (ppb)
d)
P3HT/SA
P3HT/SA-ZnO NPs
P3HT/SA-ZnO NPs (60 days storage)
P3HT/SA-ZnO NPs (1 year storage)
ΔV_T/V_T0
Biotin (ppb)

Fig. 3

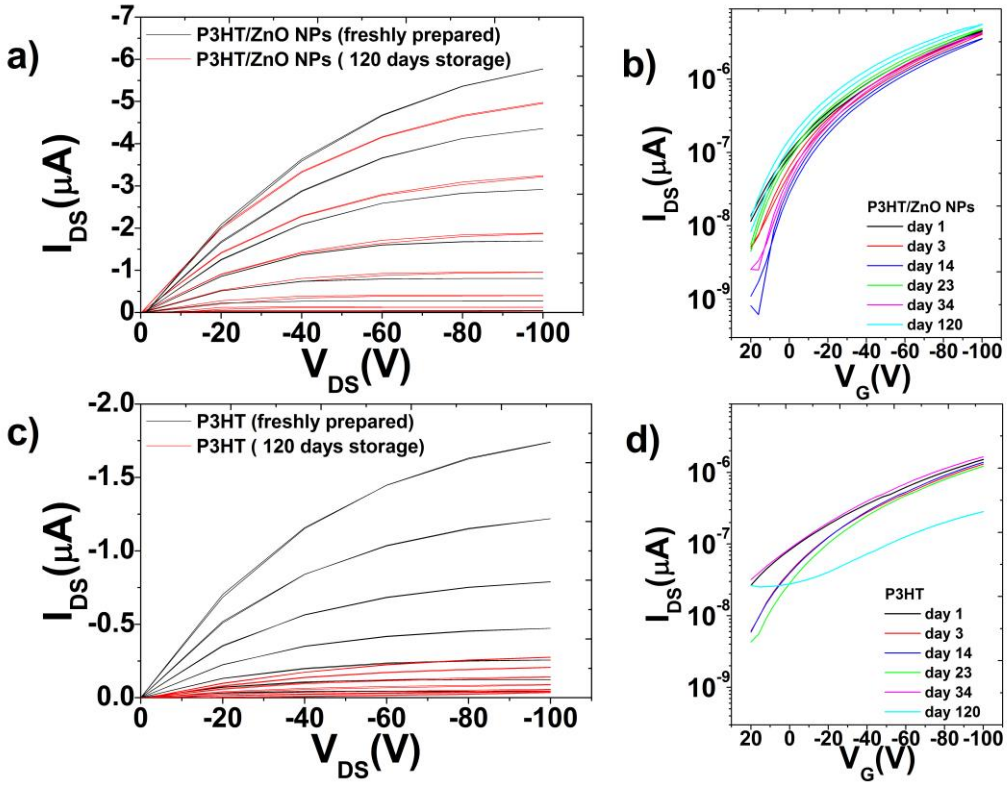
a)
P3HT/ZnO NPs (freshly prepared)
P3HT/ZnO NPs (120 days storage)
$I_{DS}(\mu A)$
$V_{DS}(V)$
b)
P3HT/ZnO NPs
day 1
day 3
day 14
day 23
day 34
day 120
$I_{DS}(\mu A)$
$V_G(V)$
c)
P3HT (freshly prepared)
P3HT (120 days storage)
$I_{DS}(\mu A)$
$V_{DS}(V)$
d)
P3HT
day 1
day 3
day 14
day 23
day 34
day 120
$I_{DS}(\mu A)$
$V_G(V)$

Fig. 4

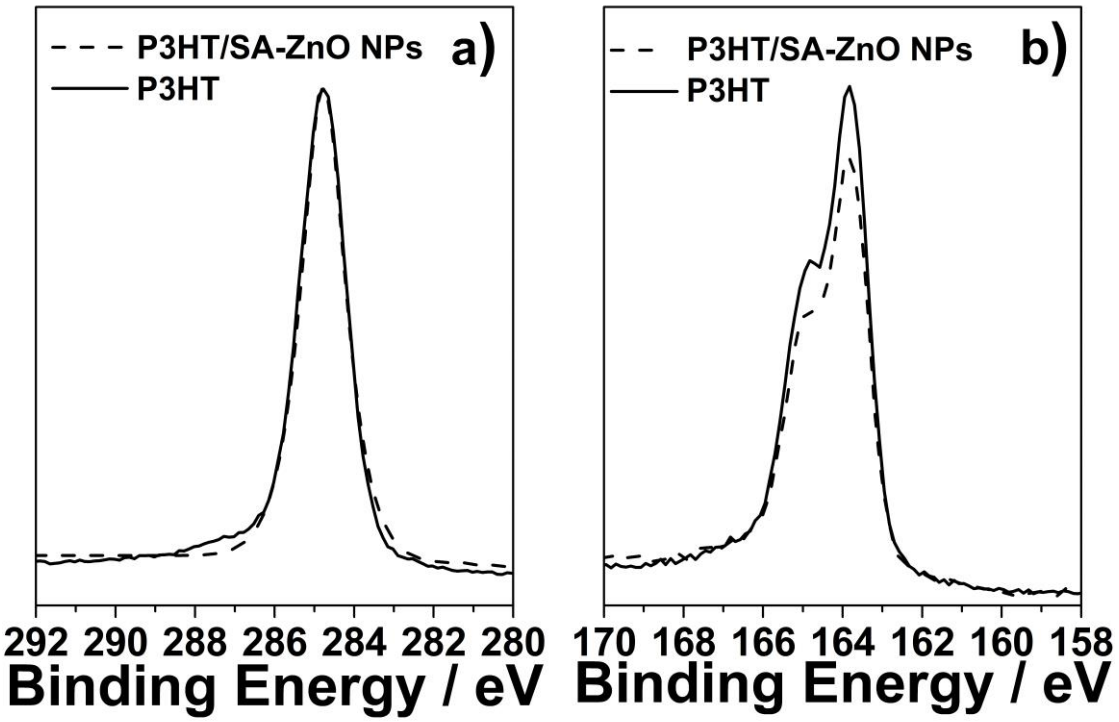
P3HT/SA-ZnO NPs
P3HT
a)
292 290 288 286 284 282 280
Binding Energy / eV
P3HT/SA-ZnO NPs
P3HT
b)
170 168 166 164 162 160 158
Binding Energy / eV

Fig. 5

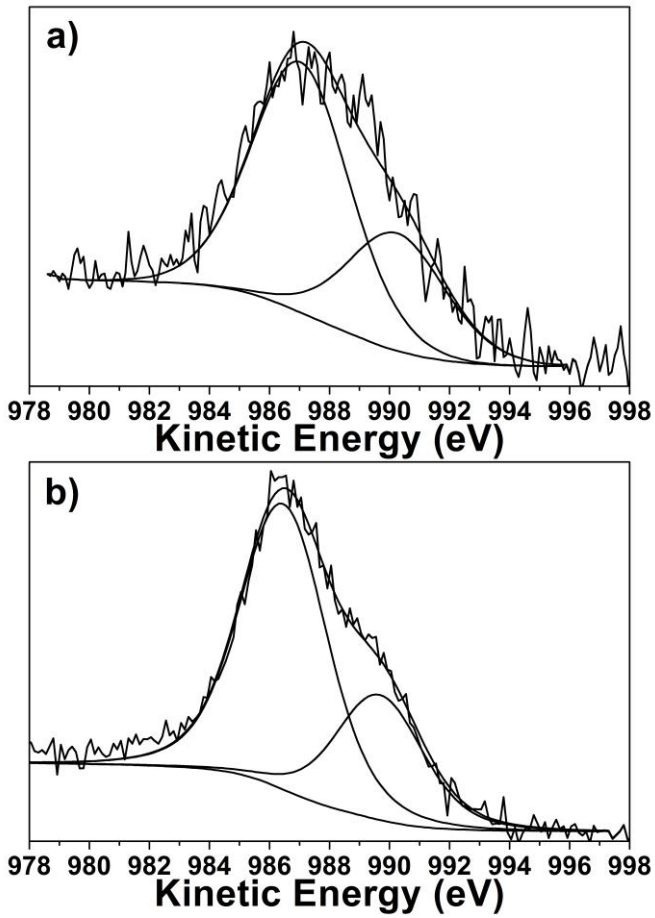
a)
978 980 982 984 986 988 990 992 994 996 998
Kinetic Energy (eV)
b)
978 980 982 984 986 988 990 992 994 996 998
Kinetic Energy (eV)

Fig. 6